Supporting Information

Porous Nb_4N_5/rGO Nanocomposite for Ultrahigh-Energy-Density Lithium-Ion Hybrid Capacitor

Shengyuan Li[†§], Ting Wang[‡§], Yunpeng Huang[†], Zengxi Wei[#], Guochun Li[†], Dickon H. L. Ng[£], Jiabiao Lian[†], Jingxia Qiu[†], Yan Zhao[†], Xiaoyan Zhang[†], Jianmin Ma*[#], and Huaming Li[†]*

[†] Institute for Energy Research, Jiangsu University, Zhenjiang 212013, P. R. China

[‡] Nanyang Environment and Water Research Institute (NEWRI), Interdisciplinary Graduate School (IGS), Nanyang Technological University, 50 Nanyang Avenue, 639798, Singapore

[#] School of Physics and Electronics, Hunan University, Changsha, 410082, P. R. China

[£] Department of Physics, The Chinese University of Hong Kong, Shatin, Hong Kong, China

[§] S. Y. Li and T. Wang contributed equally to the work.

* Corresponding author. E-mail: jblian@ujs.edu.cn (J. B.); nanoelechem@hnu.edu.cn (J. M.).

Characterization Methods. The phase and structure of the samples were confirmed by the powder X-ray diffractometer (XRD, German Bruker D8 diffractometer with Cu K_α radiation) and X-ray photoelectron spectra (XPS, Thermo Scientific ESCALAB 250Xi system with a monochromated Al K_α X-ray source 1486.6 eV). Morphology observations were performed on field emission scanning electron microscope (FE-SEM, JEOL JSM-7800F) and high-resolution transmission electron microscope (HRTEM, FEI Tecnai G^2 F30 S-Twin TEM operated at 300 kV). Nitrogen adsorption–desorption isotherms were measured on a Micromeritics Tristar II 3020 surface area analyzer at 77 K. The Brunauer–Emmett–Teller (BET) specific surface areas (S_{BET}) were calculated using the BET equation, and the pore size distributions were determined using the Barret–Joyner–Halender (BJH) method. The Fourier transform infrared (FT-IR) spectroscopy was conducted on a Thermo Scientific Nicolet iS50 FT-IR spectrometer.

Fabrication of Half-Cell and LIHC Devices. For the fabrication of anode electrodes, the active materials (the as-prepared porous Nb_4N_5 nanoparticles or Nb_4N_5/rGO nanocomposite) were mixed with super conductive carbon black (SCCB, Ketjenblack EC-600JD, Lion Corporation) and polyvinylidene fluoride (PVDF) at a weight ratio of 8:1:1, and dispersed in N-methyl-2-pyrrolidone to form a slurry. The slurry was spread and pressed on a copper foil, dried at 80 °C for 12 h under vacuum prior to be punched into 10 mm diameter electrodes with a mass loading of 1.0−1.5 mg. 2032-type coin half cells were assembled in an Ar-filled glove box, using lithium foil as the reference and counter electrode, 1M $LiPF_6$ in a 1:1 (v/v) mixture of ethylene carbonate (EC) and dimethyl carbonate (DMC) as the electrolyte, and Celgard 2400 porous polypropylene membrane as the separator. The LIHC was also assembled in coin cells by using pre-lithiated Nb_4N_5/rGO anode (galvanostatic charged-discharged for 10 cycles and ending in a lithiated state at 0.5 V under a low current density of 0.1 A g^{-1}) and commercial super conductive carbon black (SCCB) cathode in the same electrolyte. For the fabrication of cathode electrodes, 80 wt% SCCB nanopowder and 20 wt% PTFE were mixed and then rolled into thin sheets. An Al foil was used as the current collector of the cathode.

Electrochemical Measurements. Cyclic voltammetry (CV) at various scanning rates, galvanostatic charge-discharge (GCD) measurements at various current densities, and electrochemical impedance spectroscopy (EIS) measurements in the frequency from 100 kHz to 0.01 Hz were performed on a Gamry Interface 1000E Potentiostat. Cycle-life tests for half cells and hybrid full cells were conducted on a Land CT 2001A battery test system. The weight was based on the active materials, excluding PVDF or PTFE.

The specific capacitance (C, F g^{-1}), energy density (E, Wh kg^{-1}), and power density (P, W kg^{-1}) of the LIHC are calculated from the galvanostatic discharge curves at various discharge current densities according to the following equations:

$$C = I / [(dV / dt) \times m] \approx (I \Delta t) / (m \Delta V) \quad (F\ g^{-1}) \qquad (1)$$

$$E = \tfrac{1}{2}\, C\, (\Delta V)^2 / 3.6 \quad (Wh\ kg^{-1}) \qquad (2)$$

$$P = 3600\, E / \Delta t \quad (W\ kg^{-1}) \qquad (3)$$

where I is the constant discharge current (A), m is the mass of the active anode and cathode materials (g), Δt is the discharge time (s) and ΔV is the potential range (V) after IR drop.

Figure S1. Nitrogen adsorption–desorption isothermal and the BJH pore size distribution curves (inset) of porous Nb_4N_5 nanoparticle (a), Nb_4N_5/rGO nanocomposite (b), and SCCB nanopowder (c).

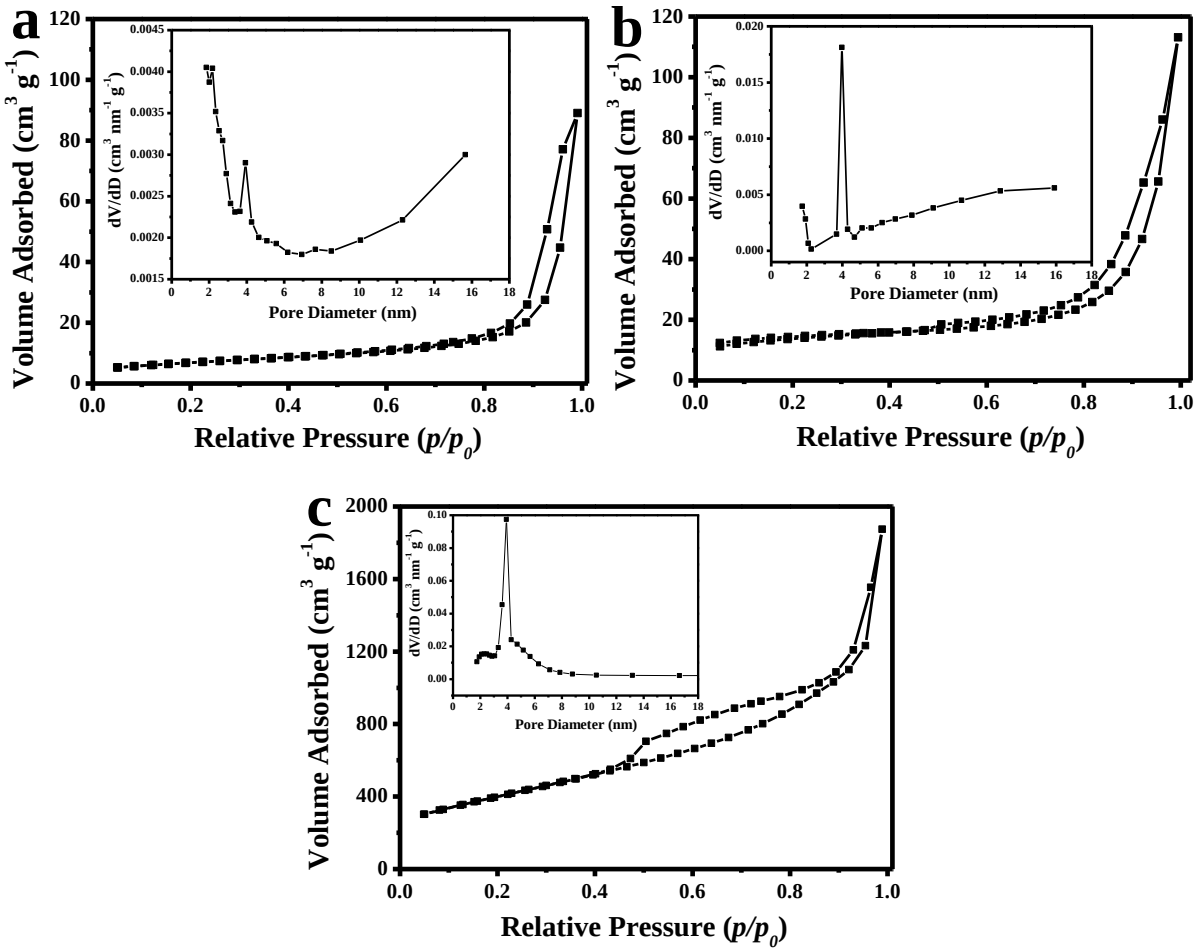

Figure S2. (a) TEM image, (b) FTIR spectrum, (c) C 1s and (d) O1s core level XPS spectra of the as-prepared GO nanosheet.

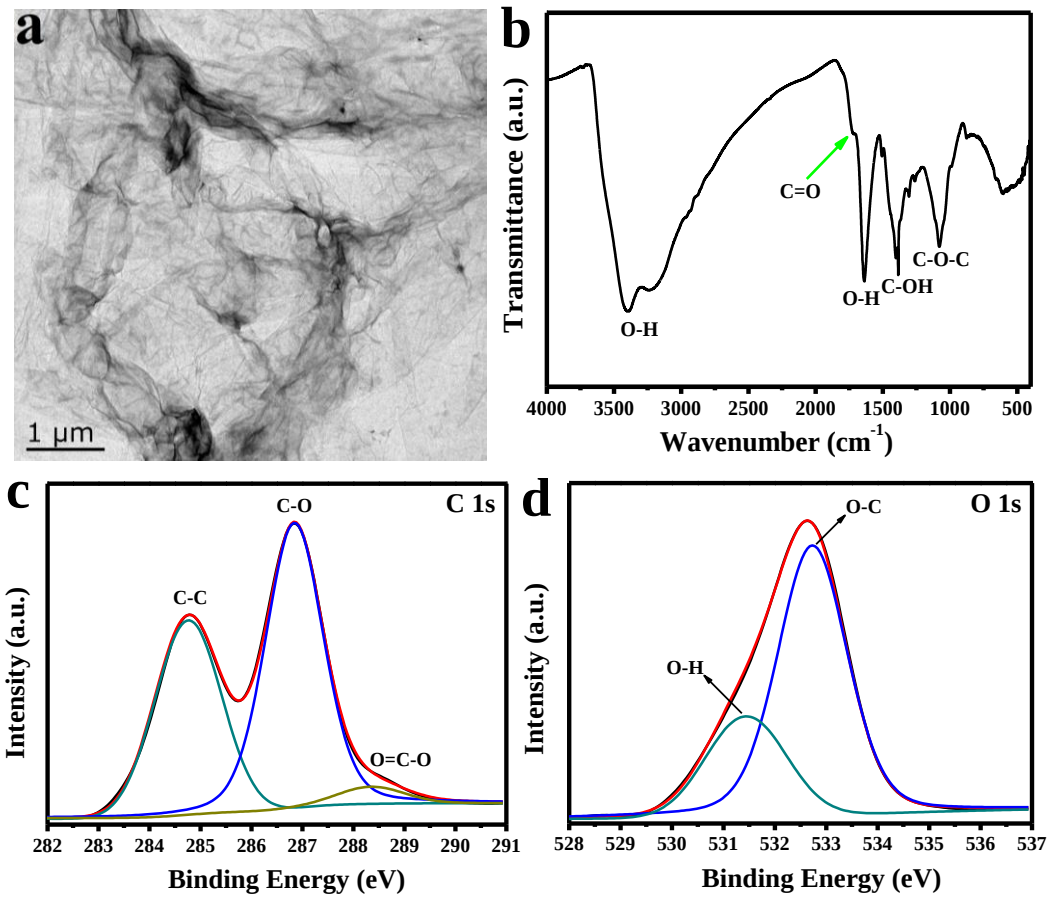

As shown in Figure S2b, the FT-IR spectrum of GO nanosheet indicates the presence of C−O−C (ν_{C-O-C} at 1080 cm^{-1}), C−OH (ν_{C-OH} at 1402 cm^{-1}), C=O in carboxylic acid and carbonyl moieties ($\nu_{C=O}$ at 1730 cm^{-1}). The broad absorption peak between 3000 and 3500 cm^{-1} is due to the presence of surface hydroxyl groups, and a peak at 1636 cm^{-1} is attributed assigned to the bending vibration of water molecules. Moreover, the XPS results (Figure S2c and S2d) are in good accordance with the FT-IR analyses, which further demonstrate that the as-prepared GO nanosheet contains many functional groups, including C−O−C, −COOH, C=O, and −OH.

Figure S3. Electrochemical performance of the SCCB nanopowder electrode in a half cell between 3.0 and 4.5 V vs. Li/Li$^+$ in the 1 M $LiPF_6$ electrolyte. (a) CV curves at different sweep rates ranging from 1.0 mV s^{-1} to 50 mV s^{-1}. (b) Galvanostatic charge-discharge curves at different current densities of 0.1−5.0 A g^{-1}. (c) Gravimetric capacitance as a function of current density. (d) Cycling performance at the current density of 1.0 A g^{-1}.

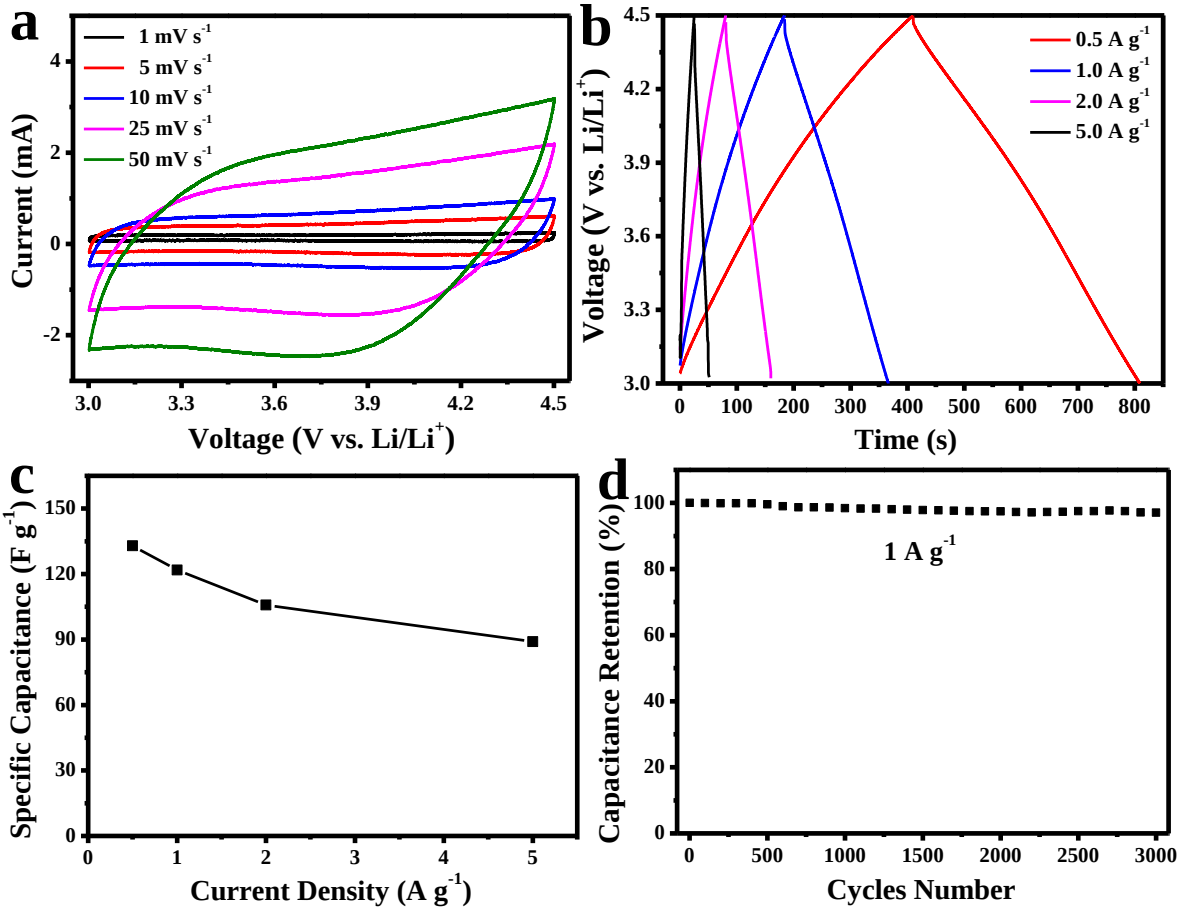

To design and assemble a high-performance LIHC, the commercial super conductive carbon black (SCCB) nanopowder with a large surface area of 1439 m^2 g^{-1} (Figure S1c) was chosen as cathode to couple with the pre-lithiated Nb_4N_5/rGO anode. Figure S3a shows the CV curves of SCCB nanopowder in the potential range of 3.0−4.5 V (vs. Li/Li$^+$) at different scanning rates from 1.0 to 50 mV s^{-1}, which exhibit typical rectangular shape, indicating its superior electrical double-layer characteristic. The galvanostatic charge-discharge (GCD) curves at various current densities (Figure S3b) exhibit excellent symmetry, revealing its good reversibility. Its specific

capacitance is calculated to be 132 F g^{-1} (corresponding to 55 mAh g^{-1}) at a current density of 0.5 A g^{-1}, and remains 89 F g^{-1} even at a high current density of 5.0 A g^{-1}, as shown in Figure S3c. More importantly, the SCCB electrode exhibits an outstanding cycling stability with 97% capacitance retention after 3000 cycles at 1.0 A g^{-1} (Figure S3d). These results reveal that the SCCB nanopowder has high specific capacitance, remarkable rate capability, and long cycle life, which is very suitable for high-performance hybrid capacitor.

In order to make full use of both electrode materials for achieving high energy and power densities, the working potential ranges of these two kinds of electrodes have to be matched and the mass ratio of the two electrode materials need to be optimized. Based on the above investigation, the Nb_4N_5/rGO-based electrode works in the potential range of 0.01−3 V (*vs.* Li/ Li^+) and the SCCB-based electrode works in the potential range of 3−4.5 V (*vs.* Li/ Li^+), thus the maximum working potential window of the LIHC could reach up to 4.5 V. On the other hand, according to the charge balance between the cathode and anode ($m_+q_+ = m_-q_-$, where q is the specific capacity, m is the mass of electrode active materials, and subscripts stand for the positive and negative electrode), the mass ratio of SCCB nanopowders to Nb_4N_5/rGO nanocomposite is optimized to be 5: 1.

Figure S4. IR drops of the as-fabricated Nb_4N_5/rGO//SCCB LIHC at various discharge current densities.

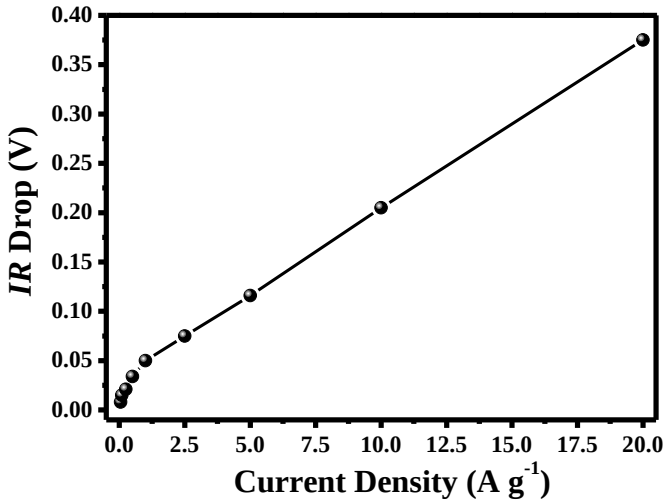

Table S1. Electrochemical performance of our Nb_4N_5/rGO//SCCB LIHC in comparison with other previously reported hybrid capacitors.

Anode//Cathode [Reference]	Potential Range (V)	Energy Density (W h kg^{-1})	Power Density (W kg^{-1})	Cycling Life
Nb_4N_5/rGO//SCCB Present work	**0.01−4.5**	**295.1**	**41250**	**92.8%@4000 cycles**
p-NbN//APDC [1]	0−4	149	45000	95%@15000 cycles
NbN/GNSs//APDC [2]	1−4	136	25000	84%@2000 cycles
NbN/NG//AC [3]	2−4	122.7	2000	81.7%@1000 cycles
3D VN−RGO//APDC [4]	0−4	162	10000	83%@1000 cycles
Nb_2O_5//AC [5]	1−3.5	95.55	5350.9	81%@1000 cycles
Nb_2O_5@C/rGO//AC [6]	1−4.3	76	20800	100%@3000 cycles
TNO@C//CFs [7]	0.8−3.2	110.4	5464	77%@1500 cycles
$TiNb_2O_7$//graphene [8]	0−3	74	7500	81.25%@3000 cycles
CC-CNTs/LTO//LFP [9]	1−2.5	125	3000	87%@1500 cycles
TiO_2/CNT//AC/CNT [10]	1−4	104	5000	71%@2000 cycles
TiO_2@EEG//EEG [11]	0−3	72	2000	68%@500 cycles
TiC//PHPNC [12]	0−4.5	101.5	67500	82%@5000 cycles
CTAB−Sn@Ti_3C_2//AC [13]	1−4	239.5	10800	71.1%@4000 cycles
CG@SF//CG [14]	1−4	121	18000	87%@2000 cycles
Fe_3O_4/G/3Dgraphene [15]	1−4	204	4600	70%@1000 cycles
MnO-C//AC [16]	0.1−4	227	2955	92.5%@3500 cycles
MnO/CNS//3D-CNS [17]	1−4	184	18000	76%@5000 cycles
MnO@GNS//HNC [18]	1−4	127	25000	76%@3000 cycles
WO_3/C//MOF-NC [19]	1.1−3.6	159.97	1736	88.3%@3000 cycles
Si/C//eAC-900 [20]	2−4.5	257	29893	79.2%@15000 cycles
SC//NPHC [21]	0.01−4.7	245.7	13846.1	83%@1000 cycles
C-NVP/CDC [22]	0−3	118	850	95%@10000 cycles
Disordered C//Graphene [23]	0−4.2	168	2432	85%@1200 cycles
BNC//BNC [24]	0−4.5	220	22500	81%@5000 cycles
ANCS//ANCS [25]	0−4.5	206	22500	86.6%@10000 cycles

References:

1. P. Y. Wang, R. T. Wang, J. W. Lang, X. Zhang, Z. K. Chen, X. B. Yan, Porous Niobium Nitride as a Capacitive Anode Material for Advanced Li-Ion Hybrid Capacitor with Superior Cycling Stability. *J. Mater. Chem. A* **2016**, *4*, 9760−9766.
2. Z. K. Chen, J. W. Lang, L. Y. Liu, L. B. Kong, Preparation of a NbN/graphene Nanocomposite by Solution Impregnation and Its Application in High-Performance Li-Ion Hybrid Capacitors. *RSC Adv.* **2017**, 7, 19967–19975.
3. M. Liu, L. X. Zhang, P. X. Han, X. Q. Han, H. P. Du, X. Y. Yue, Z. Y. Zhang, H. Zhang, G. L. Cui, Controllable Formation of Niobium Nitride/Nitrogen-Doped Graphene Nanocomposites as Anode Materials for Lithium-Ion Capacitors. *Part. Part. Syst. Charact*. **2015**, 32, 1006−1011.
4. R. T. Wang, J. W. Lang, P. Zhang, Z. Y. Lin, X. B. Yan, Fast and Large Lithium Storage in 3D Porous VN Nanowires-Graphene Composite as a Superior Anode Toward High-Performance Hybrid Supercapacitors. *Adv. Funct. Mater*. **2015**, *25*, 2270−2278.
5. B. H. Deng, T. Y. Lei, W. H. Zhu, L. Xiao, J. P. Liu, In-Plane Assembled Orthorhombic Nb_2O_5 Nanorod Films with High-Rate Li^+ Intercalation for High-Performance Flexible Li-Ion Capacitors. *Adv. Funct. Mater.* **2018**, 28, 1704330.
6. E. Lim, C. Jo, M. S. Kim, M. H. Kim, J. Chun, H. Kim, J. Park, K. C. Roh, K. Kang, S. Yoon, High-Performance Sodium-Ion Hybrid Supercapacitor Based on Nb_2O_5@Carbon Core-Shell Nanoparticles and Reduced Graphene Oxide Nanocomposites. *Adv. Funct. Mater.* **2016**, *26*, 3711−3719.
7. X. F. Wang, G. Z. Shen, Intercalation Pseudo-capacitive $TiNb_2O_7$@Carbon Electrode for High-Performance Lithium Ion Hybrid Electrochemical Supercapacitors with Ultrahigh Energy Density. *Nano Energy* **2015**, *15*, 104−115.
8. H. S. Li, L. F. Shen, J. Wang, S. Fang, Y. X. Zhang, H. Dou, X. G. Zhang, Three-Dimensionally Ordered Porous $TiNb_2O_7$ Nanotubes: A Superior Anode Material for Next Generation Hybrid Supercapacitors. *J. Mater. Chem. A* **2015**, *3*, 16785−16790.
9. Z. J. Yao, X. H Xia, C. A. Zhou, Y. Zhong, Y. D. Wang, S. J. Deng, W. Q. Wang, X. L. Wang, J. P. Tu, Smart Construction of Integrated CNTs/$Li_4Ti_5O_{12}$ Core/Shell Arrays with Superior High-Rate Performance for Application in Lithium-Ion Batteries. *Adv. Sci.* **2018**, *5*, 1700786.
10. L. F. Que, F. D. Yu, Z. B. Wang, D. M. Gu, Pseudocapacitance of TiO_{2-x}/CNT Anodes for High-Performance Quasi-Solid-State Li-Ion and Na-Ion Capacitors. *Small* **2018**, *14*, 1704508.
11. F. X. Wang, C. Wang, Y. J. Zhao, Z. C. Liu, Z. Chang, L. J. Fu, Y. S. Zhu, Y. P. Wu, D. Y. Zhao, A Quasi-Solid-State Li-Ion Capacitor Based on Porous TiO_2 Hollow Microspheres Wrapped with Graphene Nanosheets. *Small* **2016**, *12*, 6207−6213.
12. H. W. Wang, Y. Zhang, H. X. Ang, Y. Q. Zhang, H. T. Tan, Y. F. Zhang, Y. Y. Guo, J. B. Franklin, X. L. Wu, M. Srinivasan, H. J. Fan, Q. Y. Yan, A High Energy Lithium-Ion Capacitor by Integration of a 3D Interconnected Titanium Carbide Nanoparticle Chain Anode with a Pyridine-Derived Porous Nitrogen-Doped Carbon Cathode. *Adv. Funct. Mater.* **2016**, *26*, 3082−3093.
13. J. M. Luo, W. K. Zhang, H. D. Yuan, C. B. Jin, L. Y. Zhang, H. Huang, C. Liang, Y. Xia, J. Zhang, Y. P. Gan, X. Y. Tao, Pillared Structure Design of MXene with Ultralarge Interlayer Spacing for High-Performance Lithium-Ion Capacitors. *ACS Nano* **2017**, *11*, 2459−2469.

14. E. Kim, H. Kim, B. J. Park, Y. H. Han, J. H. Park, J. Cho, S. S. Lee, J. G. Son, Etching-Assisted Crumpled Graphene Wrapped Spiky Iron Oxide Particles for High-Performance Li-Ion Hybrid Supercapacitor. *Small* **2018**, *14*, 1704209.
15. F. Zhang, T. F. Zhang, X. Yang, L. Zhang, K. Leng, Y. Huang, Y. S. Chen, A High-Performance Supercapacitor-Battery Hybrid Energy Storage Device Based on Graphene-Enhanced Electrode Materials with Ultrahigh Energy Density. *Energy Environ. Sci.* **2013**, *6*, 1623−1632.
16. C. F. Liu, C. K. Zhang, H. Q. Song, C. P. Zhang, Y. G. Liu, X. H. Nan, G. Z. Cao, Mesocrystal MnO Cubes as Anode for Li-Ion Capacitors. *Nano Energy* **2016**, *22*, 290−300.
17. H. L. Wang, Z. W. Xu, Z. Li, K. Cui, J. Ding, A. Kohandehghan, X. H. Tan, B. Zahiri, B. C. Olsen, C. M. B. Holt, D. Mitlin, Hybrid Device Employing Three-Dimensional Arrays of MnO in Carbon Nanosheets Bridges Battery-Supercapacitor Divide. *Nano Lett.* **2014**, *14*, 1987−1994.
18. M. Yang, Y. R. Zhong, J. J. Ren, X. L. Zhou, J. P. Wei, Z. Zhou, Fabrication of High-Power Li-Ion Hybrid Supercapacitors by Enhancing the Exterior Surface Charge Storage. *Adv. Energy Mater.* **2015**, *5*, 1500550.
19. J. Xu, Y. Y. Li, L. Wang, Q. F. Cai, Q. W. Li, B. Gao, X. M. Zhang, K. F. Huo, P. K. Chu, High-Energy Lithium-Ion Hybrid Supercapacitors Composed of Hierarchical Urchin-Like WO_3/C Anodes and MOF-Derived Polyhedral Hollow Carbon Cathodes. *Nanoscale* **2016**, *8*, 16761−16768.
20. B. Li, F. Dai, Q. F. Xiao, L. Yang, J. M. Shen, C. M. Zhang, M. Cai, Activated Carbon from Biomass Transfer for High-Energy Density Lithium-Ion Supercapacitors. *Adv. Energy Mater.* **2016**, *6*, 1600802.
21. S. H. Chen, J. Wang, L. Fan, R. F. Ma, E. J. Zhang, Q. Liu, B. Lu, An Ultrafast Rechargeable Hybrid Sodium-Based Dual-Ion Capacitor Based on Hard Carbon Cathodes. *Adv. Energy Mater.* **2018**, *8*, 1800140.
22. R. Thangavel, K. Kaliyappan, K. Kang, X. L. Sun, Y. S. Lee, Going Beyond Lithium Hybrid Capacitors: Proposing a New High-Performing Sodium Hybrid Capacitor System for Next-Generation Hybrid Vehicles Made with Bio-Inspired Activated Carbon. *Adv. Energy Mater.* **2016**, *6*, 1502199.
23. F. Wang, X. Wang, Z. Chang, X. Wu, X. Liu, L. Fu, Y. Zhu, Y. Wu, W. Huang, A Quasi-Solid-State Sodium-Ion Capacitor with High Energy Density. *Adv. Mater.* **2015**, *27*, 6962−6968.
24. Q. Y. Xia, H. Yang, M. Wang, M. Yang, Q. B. Guo, L. M. Wan, H. Xia, Y. Yu, High Energy and High Power Lithium-Ion Capacitors Based on Boron and Nitrogen Dual-Doped 3D Carbon Nanofibers as Both Cathode and Anode. *Adv. Energy Mater.* **2017**, *7*, 1701336.
25. F. Sun, X. Y. Liu, H. B. Wu, L. J. Wang, J. H. Gao, H. X. Li, Y. F. Lu, In Situ High-Level Nitrogen Doping into Carbon Nanospheres and Boosting of Capacitive Charge Storage in Both Anode and Cathode for a High-Energy 4.5 V Full-Carbon Lithium-Ion Capacitor. *Nano Lett.* **2018**, *18*, 3368−3376.